Precise optical modeling of blue light-emitting diodes by Monte Carlo ray-tracing

Zongyuan Liu,[1,2] Kai Wang,[1] Xiaobing Luo,[1] and Sheng Liu,[1,2,*]

[1]*Wuhan National Laboratory for Optoelectronics, Huazhong University of Science and Technology, Wuhan 430074, China*

[2]*School of Mechanical Science and Engineering, Huazhong University of Science and Technology, Wuhan 430074, China*

**victor_liu63@126.com*

Abstract: Precise optical modeling of blue light-emitting diodes (LEDs) is constructed by reasonable optical parameters and Monte Carlo ray-tracing with the capability of precisely predicting light extraction and radiation pattern for both bare LED and packaged LED. Refractive indices and absorption coefficients of LED materials are determined by abundant references and comparisons between simulations and experiments. Surface roughness is considered in the optical model to improve the simulation precision. The simulation precisions are excellent for both bare blue LEDs (>96.5% for light extraction and >99% for radiation pattern) and packaged blue LEDs (>98.5% for both light extraction and radiation pattern).

OCIS codes: (230.3670) Light-emitting diodes; (350.4600) Optical engineering.

References and links

1. C.-C. Sun, C.-Y. Chen, H.-Y. He, C.-C. Chen, W.-T. Chien, T.-X. Lee, and T.-H. Yang, "Precise optical modeling for silicate-based white LEDs," Opt. Express **16**(24), 20060–20066 (2008).
2. C.-C. Sun, W.-T. Chien, I. Moreno, C.-C. Hsieh, and Y.-C. Lo, "Analysis of the far-field region of LEDs," Opt. Express **17**(16), 13918–13927 (2009).
3. Z. Y. Liu, S. Liu, K. Wang, and X. B. Luo, "Optical analysis of color distribution in white LEDs with various packaging methods," IEEE Photon. Technol. Lett. **20**(24), 2027–2029 (2008).
4. Z. Y. Liu, S. Liu, K. Wang, and X. B. Luo, "Optical analysis of phosphor's location for high-power light-emitting diodes," IEEE Trans. Device Mater. Reliab. **9**(1), 65–73 (2009).
5. Z. Y. Liu, S. Liu, K. Wang, and X. B. Luo, "Studies on optical consistency of white LEDs affected by phosphor thickness and concentration using optical simulation," IEEE Trans. Compon. Packag. Tech. (Accepted).
6. J. K. Kim, H. Luo, E. F. Schubert, J. Cho, C. Sone, and Y. Park, "Strongly enhanced phosphor efficiency in GaInN white light-emitting diodes using remote phosphor configuration and diffuse reflector cup," Jpn. J. Appl. Phys. **44**(21), L649–L651 (2005).
7. H. Luo, J. K. Kim, E. F. Schubert, J. Cho, C. Sone, and Y. Park, "Analysis of high-power packages for phosphor-based white-light-emitting diodes," Appl. Phys. Lett. **86**(24), 243505 (2005).
8. N. T. Tran, and F. G. Shi, "Studies of phosphor concentration and thickness for phosphor-based white light-emitting-diodes," J. Lightwave Technol. **26**(21), 3556–3559 (2008).
9. C.-C. Sun, T.-X. Lee, S.-H. Ma, Y.-L. Lee, and S.-M. Huang, "Precise optical modeling for LED lighting verified by cross correlation in the midfield region," Opt. Lett. **31**(14), 2193–2195 (2006).
10. S. J. Lee, "Analysis of light-emitting diodes by Monte Carlo photon simulation," Appl. Opt. **40**(9), 1427–1437 (2001).
11. T.-X. Lee, C.-Y. Lin, S.-H. Ma, and C.-C. Sun, "Analysis of position-dependent light extraction of GaN-based LEDs," Opt. Express **13**(11), 4175–4179 (2005).
12. T.-X. Lee, K.-F. Gao, W.-T. Chien, and C.-C. Sun, "Light extraction analysis of GaN-based light-emitting diodes with surface texture and/or patterned substrate," Opt. Express **15**(11), 6670–6676 (2007).
13. H. Wang, J. H. Ryu, K. S. Lee, C. H. Tan, L. H. Jin, S. M. Li, C. H. Hong, Y. H. Cho, and S. H. Liu, "Active packing method for blue light-emitting diodes with photosensitive polymerization: formation of self-focusing encapsulates," Opt. Express **16**(6), 3680–3685 (2008).
14. A. Borbely, and S. G. Johnson, "Performance of phosphor-coated LED optics in ray trace simulations," in *Fourth International Conference on Solid State Lighting*, (SPIE, 2004), 266–273.
15. T. Peng, and J. Piprek, "Refractive index of AlGaInN alloys," Electron. Lett. **32**(24), 2285–2286 (1996).
16. G. M. Laws, E. C. Larkins, I. Harrison, C. Molloy, and D. Somerford, "Improved refractive index formulas for the $Al_xGa_{1-x}N$ and $In_yGa_{1-y}N$ alloys," J. Appl. Phys. **89**(2), 1108–1115 (2001).
17. F. Yun, M. A. Reshchikov, L. He, T. King, H. Morkoc, S. W. Novak, and L. Wei, "Energy band bowing parameter in Al[sub x]Ga[sub 1 - x]N alloys," J. Appl. Phys. **92**(8), 4837–4839 (2002).

#122383 - $15.00 USD Received 3 Feb 2010; revised 29 Mar 2010; accepted 5 Apr 2010; published 21 Apr 2010

18. W. Walukiewicz, S. X. Li, J. Wu, K. M. Yu, J. W. Ager, E. E. Haller, H. Lu, and W. J. Schaff, "Optical properties and electronic structure of InN and In-rich group III-nitride alloys," J. Cryst. Growth **269**(1), 119–127 (2004).
19. M. Anani, H. Abid, Z. Chama, C. Mathieu, A. Sayede, and B. Khelifa, "$In_xGa_{1-x}N$ refractive index calculations," Microelectron. J. **38**(2), 262–266 (2007).
20. A. B. Djurišić, and E. H. Li, "Modeling the optical constants of hexagonal GaN, InN, and AlN," J. Appl. Phys. **85**(5), 2848–2853 (1999).
21. L. F. Jiang, W. Z. Shen, H. F. Yang, H. Ogawa, and Q. X. Guo, "Temperature effects on optical properties of InN thin films," Appl. Phys. A: Mater. Sci. Process **78**(1), 89–93 (2004).
22. H. Ahn, C. H. Shen, C. L. Wu, and S. Gwo, "Spectroscopic ellipsometry study of wurtzite InN epitaxial films on Si(111) with varied carrier concentrations," Appl. Phys. Lett. **86**(20), 201905 (2005).
23. R. R. Lieten, S. Degroote, M. Leys, J. Derluyn, M. Kuijk, and G. Borghs, "Growth of InN on Ge(1 1 1) by molecular beam epitaxy using a GaN buffer," J. Cryst. Growth **310**(6), 1132–1136 (2008).
24. M. J. Bergmann, and J. H. C. Casey, "Optical-field calculations for lossy multiple-layer $Al_xGa_{1-x}N/In_xGa_{1-x}N$ laser diodes," J. Appl. Phys. **84**(3), 1196–1203 (1998).
25. I. H. Malitson, and M. J. Dodge, "Refractive index and birefringence of synthetic sapphire," in *1972 Annual Meeting of the Optical Society of America*, (Optical Soc. America, 1972), 78.
26. H. El Rhaleb, E. Benamar, M. Rami, J. P. Roger, A. Hakam, and A. Ennaoui, "Spectroscopic ellipsometry studies of index profile of indium tin oxide films prepared by spray pyrolysis," Appl. Surf. Sci. **201**(1-4), 138–145 (2002).
27. Y. S. Jung, "Spectroscopic ellipsometry studies on the optical constants of indium tin oxide films deposited under various sputtering conditions," Thin Solid Films **467**(1-2), 36–42 (2004).
28. J. Zhou, "Indium tin oxide (ITO) deposition, patterning, and Schottky contact fabrication," (Rochester Insititute of Technology, 2005).
29. H. N. Cui, V. Teixeira, L. J. Meng, R. Martins, and E. Fortunato, "Influence of oxygen/argon pressure ratio on the morphology, optical and electrical properties of ITO thin films deposited at room temperature," Vacuum **82**(12), 1507–1511 (2008).
30. O. Ambacher, W. Rieger, P. Ansmann, H. Angerer, T. D. Moustakas, and M. Stutzmann, "Sub-bandgap absorption of gallium nitride determined by photothermal deflection spectroscopy," Solid State Commun. **97**(5), 365–370 (1996).
31. G. Bentoumi, A. Deneuville, B. Beaumont, and P. Gibart, "Influence of Si doping level on the Raman and IR reflectivity spectra and optical absorption spectrum of GaN," Mater. Sci. Eng. B **50**(1-3), 142–147 (1997).
32. D. Brunner, H. Angerer, E. Bustarret, F. Freudenberg, R. Hopler, R. Dimitrov, O. Ambacher, and M. Stutzmann, "Optical constants of epitaxial AlGaN films and their temperature dependence," J. Appl. Phys. **82**(10), 5090–5096 (1997).
33. G. Yu, G. Wang, H. Ishikawa, M. Umeno, T. Soga, T. Egawa, J. Watanabe, and T. Jimbo, "Optical properties of wurtzite structure GaN on sapphire around fundamental absorption edge (0.78–4.77 eV) by spectroscopic ellipsometry and the optical transmission method," Appl. Phys. Lett. **70**(24), 3209–3211 (1997).
34. H. Ye, G. W. Wicks, and P. M. Fauchet, "Hot electron relaxation time in GaN," Appl. Phys. Lett. **74**(5), 711–713 (1999).
35. H. Ye, G. W. Wicks, and P. M. Fauchet, "Hot hole relaxation dynamics in p-GaN," Appl. Phys. Lett. **77**(8), 1185–1187 (2000).
36. S.-S. Schad, B. Neubert, C. Eichler, M. Scherer, F. Habel, M. Seyboth, F. Scholz, D. Hofstetter, P. Unger, W. Schmid, C. Karnutsch, and K. Streubel, "Absorption and Light Scattering in InGaN-on-Sapphire- and AlGaInP-Based Light-Emitting Diodes," J. Lightwave Technol. **22**(10), 2323–2332 (2004).
37. H. Hasegawa, Y. Kamimura, K. Edagawa, and I. Yonenaga, "Dislocation-related optical absorption in plastically deformed GaN," J. Appl. Phys. **102**, 026103 (2007).
38. Y. Lelikov, N. Bochkareva, R. Gorbunov, I. Martynov, Y. Rebane, D. Tarkin, and Y. Shreter, "Measurement of the absorption coefficient for light laterally propagating in light-emitting diode structures with In0.2Ga0.8N/GaN quantum wells," Semiconductors **42**(11), 1342–1345 (2008).
39. Y. Oshima, T. Suzuki, T. Eri, Y. Kawaguchi, K. Watanabe, M. Shibata, and T. Mishima, "Thermal and optical properties of bulk GaN crystals fabricated through hydride vapor phase epitaxy with void-assisted separation," J. Appl. Phys. **98**(10), 103509 (2005).
40. F. Omnes, N. Marenco, S. Haffouz, H. Lahreche, P. de Mierry, B. Beaumont, P. Hageman, E. Monroy, F. Calle, and E. Munoz, "Low pressure MOVPE grown AlGaN for UV photodetector applications," Mater. Sci. Eng. B **59**(1-3), 401–406 (1999).
41. R. W. Martin, P. G. Middleton, K. P. O'Donnell, and W. Van der Stricht, "Exciton localization and the Stokes' shift in InGaN epilayers," Appl. Phys. Lett. **74**(2), 263–265 (1999).
42. K. P. O'Donnell, R. W. Martin, and P. G. Middleton, "Origin of Luminescence from InGaN Diodes," Phys. Rev. Lett. **82**(1), 237–240 (1999).
43. K. P. O'Donnell, R. W. Martin, P. G. Middleton, S. C. Bayliss, I. Fletcher, W. Van der Stricht, P. Demeester, and I. Moerman, "Spectroscopy and microscopy of localised and delocalised excitons in InGaN-based light emitting diodes and epilayers," Mater. Sci. Eng. B **59**(1-3), 288–291 (1999).
44. H. C. Yang, P. F. Kuo, T. Y. Lin, Y. F. Chen, K. H. Chen, L. C. Chen, and J.-I. Chyi, "Mechanism of luminescence in InGaN/GaN multiple quantum wells," Appl. Phys. Lett. **76**(25), 3712–3714 (2000).
45. J. A. Davidson, P. Dawson, T. Wang, T. Sugahara, J. W. Orton, and S. Sakai, "Photoluminescence studies of InGaN/GaN multi-quantum wells," Semicond. Sci. Technol. **15**(6), 497–505 (2000).

#122383 - $15.00 USD Received 3 Feb 2010; revised 29 Mar 2010; accepted 5 Apr 2010; published 21 Apr 2010

46. J. Kvietkova, L. Siozade, P. Disseix, A. Vasson, J. Leymarie, B. Damilano, N. Grandjean, and J. Massies, "Optical Investigations and Absorption Coefficient Determination of InGaN/GaN Quantum Wells," Phys. Status Solidi **190**(1), 135–140 (2002).
47. Z. C. Feng, J. Chen, H. Tsai, J. Yang, P. Li, C. Wetzel, T. Detchprohm, J. Nelson, and I. T. Ferguson, "Optical and structural investigation on InGaN/GaN multiple quantum well light-emitting diodes grown on sapphire by metalorganic chemical vapor deposition," in *Sixth International Conference on Solid State Lighting*, (SPIE, 2006), 63370D.
48. Y. Takeda, D. Takagi, T. Sano, S. Tabata, N. Kobayashi, Q. Shen, T. Toyoda, J. Yamamoto, Y. Ban, and K. Matsumoto, "Room-temperature absorption edge of InGaN/GaN quantum wells characterized by photoacoustic measurement," Jpn. J. Appl. Phys. **47**(12), 8805–8807 (2008).
49. H. E. Bennett, and J. O. Porteus, "Relation Between Surface Roughness and Specular Reflectance at Normal Incidence," J. Opt. Soc. Am. **51**(2), 123–129 (1961).
50. K. H. Guenther, P. G. Wierer, and J. M. Bennett, "Surface roughness measurements of low-scatter mirrors and roughness standards," Appl. Opt. **23**(21), 3820–3836 (1984).
51. X. A. Cao, J. A. Teetsov, F. Shahedipour-Sandvik, and S. D. Arthur, "Microstructural origin of leakage current in GaN/InGaN light-emitting diodes," J. Cryst. Growth **264**(1-3), 172–177 (2004).
52. D. Lu, D. I. Florescu, D. S. Lee, V. Merai, J. C. Ramer, A. Parekh, and E. A. Armour, "Sapphire substrate misorientation effects on GaN nucleation layer properties," J. Cryst. Growth **272**(1-4), 353–359 (2004).
53. Y. Xing, J. Han, J. Deng, J. Li, C. Xu, and G. Shen, "Investigation of GaN layer grown on different low misoriented sapphire by MOCVD," Appl. Surf. Sci. **255**(12), 6121–6124 (2009).
54. H. S. Kim, and D. D. Martin, "Surface properties of GaN fabricated by laser lift-off and ICP etching," J. Korean Phys. Soc. **40**, 567–571 (2002).
55. C.-F. Chu, F.-I. Lai, J.-T. Chu, C.-C. Yu, C.-F. Lin, H.-C. Kuo, and S. C. Wang, "Study of GaN light-emitting diodes fabricated by laser lift-off technique," J. Appl. Phys. **95**(8), 3916–3922 (2004).
56. H. K. Cho, S.-K. Kim, and J. S. Lee, "An improved non-alloyed ohmic contact Cr/Ni/Au to n-type GaN with surface treatment," J. Phys. D Appl. Phys. **41**(17), 175107 (2008).
57. P. Koteswara Rao, and V. Rajagopal Reddy, "Effect of annealing temperature on electrical and structural properties of transparent indium tin oxide electrode to n-type GaN," Mater. Chem. Phys. **114**(2-3), 821–826 (2009).
58. D. Raoufi, "Morphological characterization of ITO thin films surfaces," Appl. Surf. Sci. **255**(6), 3682–3686 (2009).
59. H. Zhu, L. A. Tessaroto, R. Sabia, V. A. Greenhut, M. Smith, and D. E. Niesz, "Chemical mechanical polishing (CMP) anisotropy in sapphire," Appl. Surf. Sci. **236**(1-4), 120–130 (2004).
60. S. Zhou, and S. Liu, "Study on sapphire removal for thin-film LEDs fabrication using CMP and dry etching," Appl. Surf. Sci. **255**(23), 9469–9473 (2009).
61. V. E. Asadchikov, A. Duparré, S. Jakobs, A. Y. Karabekov, I. V. Kozhevnikov, and Y. S. Krivonosov, "Comparative Study of the Roughness of Optical Surfaces and Thin Films by use of X-Ray Scattering and Atomic Force Microscopy," Appl. Opt. **38**(4), 684–691 (1999).
62. S. Jakobs, A. Duparré, and H. Truckenbrodt, "Interfacial roughness and related scatter in ultraviolet optical coatings: a systematic experimental approach," Appl. Opt. **37**(7), 1180–1193 (1998).
63. J. C. Stover, *Optical scattering: measurement and analysis* (SPIE, Bellingham, USA, 1995).
64. A. A. Maradudin, *Light scattering and nanoscale surface roughness* (Springer, Irvine, USA, 2007).
65. J. Ferré-Borrull, A. Duparre, and E. Quesnel, "Procedure to characterize microroughness of optical thin films: application to ion-beam-sputtered vacuum-ultraviolet coatings," Appl. Opt. **40**(13), 2190–2199 (2001).
66. M. Senthilkumar, N. K. Sahoo, S. Thakur, and R. B. Tokas, "Characterization of microroughness parameters in gadolinium oxide thin films: A study based on extended power spectral density analyses," Appl. Surf. Sci. **252**(5), 1608–1619 (2005).
67. P. B. Johnson, and R. W. Christy, "Optical Constants of the Noble Metals," Phys. Rev. B **6**(12), 4370–4379 (1972).
68. T. Fujii, Y. Gao, R. Sharma, E. L. Hu, S. P. DenBaars, and S. Nakamura, "Increase in the extraction efficiency of GaN-based light-emitting diodes via surface roughening," Appl. Phys. Lett. **84**(6), 855–857 (2004).
69. I. Moreno, D. Bermúdez, and M. Avendaño-Alejo, "Light-emitting diode spherical packages: an equation for the light transmission efficiency," Appl. Opt. **49**(1), 12–20 (2010).

1. Introduction

A precise optical modeling of blue light-emitting diodes (LEDs) is critical for the study of optical issues such as light extraction, radiation pattern, and spatial color uniformity in the packaging co-design of phosphor-converted LEDs [1–8]. Previous studies have presented some reasonable optical models of LEDs by simplification of chip structures and optical properties of chip materials [1,2,4,5,9–12]. These studies normally simulate LEDs by Monte Carlo ray-tracing to compatible with the packaging modeling. Generally, three approaches are adopted. The first approach treats the LED as a homogeneous material and defines blue light to be emitted from its external surfaces, mainly from the top surface with Lambertian pattern [2,13]. In the second approach, the LED is composed of multiple layers with different

#122383 - $15.00 USD Received 3 Feb 2010; revised 29 Mar 2010; accepted 5 Apr 2010; published 21 Apr 2010

refractive indices and similar absorptions, and the blue light is randomly emitted from the active layer [4,5,10,14]. The third approach applies similar settings as those of the second approach except the absorption model, in which only the active layer absorbs light with very high absorption coefficient [1,9,11,12]. Since the first approach has difficulty showing the change of light escaping cone of the chip from bare LED to packaged LED, the second and third approaches are more widely used in the packaging modeling of white LEDs.

An increasing concern for the second and the third approaches is whether they are precise enough to predict the optical performance for both bare LED and packaged LED. Realization of precise optical modeling normally requires the simulation result to approximate the experimental result by adjustment of the optical parameters. But the adjustment should be physically reasonable. The optical parameters used in previous optical models are not clear enough and lack of sufficient references, especially for the absorption coefficients. Therefore, other researchers have difficulty improving previous studies. In addition, as far as we know, a clear comparison including light extraction and radiation pattern is not given for both bare LED and packaged LED by simulation and experiment. The verified optical parameters used for bare LED may not be practicable for packaged LED. Finally, the surface morphology is not adequately considered in previous studies. The wave guide mode of photons in LED causes strong dependence of light extraction on the surface roughness.

Therefore, this study tries to present a precise optical modeling of blue LEDs by taking into account the three issues above. Detail investigations of refractive indices and absorptions of LED materials are given in below by summarizing the references. Surface roughness is applied into LED model by introducing bidirectional scattering distribution function (BSDF). Finally, simulation results of bare and packaged LEDs are compared with experimental results to show the feasibility of our LED modeling.

2. Optical characterizations of layers of blue LEDs

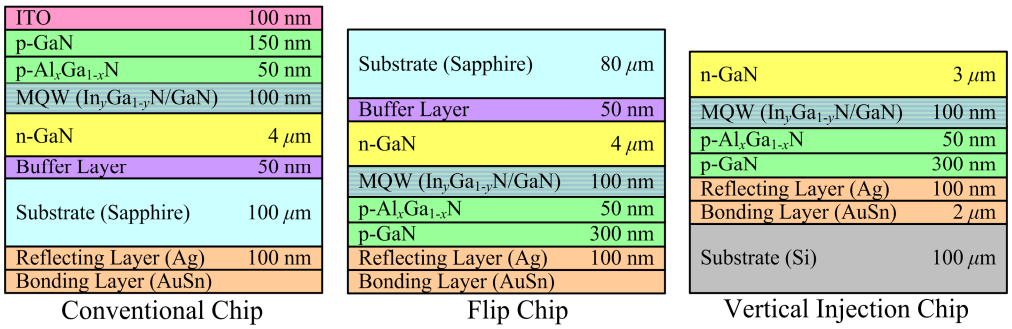

Fig. 1. Schematics of typical structures of three blue LEDs.

Figure 1 shows three typical GaN based blue LED structures that will be studied in this express. Thicknesses and composites of LED materials in each structure are given. In conventional chip, a current spreading layer fabricated by Indium Tin Oxide (ITO) is considered. In vertical injection chip, buffer layer is removed and thickness of n-GaN is thinner than that of other two chips due to the laser lift-off process and following reactive ion etching (RIE) process. Thinner p-GaN in conventional chip is to provide lower resistance, and thicker p-GaN in flip chip and vertical injection chip is to improve the mechanical strength. The chip sizes are all 1 × 1 mm to refer to high power LEDs. For simplicity, electrode pattern is not considered.

2.1 Refractive indices of blue LED materials

In visible spectra, refractive index $n(hv)$ of $Al_xGa_{1-x}N$ normally has a relationship with its bandgap E_g as [15,16]:

#122383 - $15.00 USD Received 3 Feb 2010; revised 29 Mar 2010; accepted 5 Apr 2010; published 21 Apr 2010

$$n(h\nu) = \left\{ a(h\nu / E_g)^{-2} \left[2 - (1 + h\nu / E_g)^{0.5} - (1 - h\nu / E_g)^{0.5} \right] + b \right\}^{0.5} \quad (1)$$

where h is Planck constant, ν is light frequency, a and b are fitting parameters varying with molar fraction x. When x changes to 0, $n(h\nu)$ of Eq. (1) will be refractive index of GaN. From [16], E_g, a, and b are:

$$E_g(x) = 3.45(1-x) + 6.13x - 1.3x(1-x) \quad (2)$$

$$a(x) = 9.82661 - 8.21608x - 31.5902x^2 \quad (3)$$

$$b(x) = 2.73591 + 0.84249x - 6.29321x^2 \quad (4)$$

Generally, E_g of $Al_xGa_{1-x}N$ is varied by the fabrication procedure, sample quality and temperature. Results of Eq. (2) are compatible with recent experimental studies on E_g of $Al_xGa_{1-x}N$ [17,18], and believed to be feasible for the calculation of $n(h\nu)$ of $Al_xGa_{1-x}N$.

Determination of refractive index of $In_yGa_{1-y}N$ is more complicated due to the poor sample quality by phase separation of In. An empirical formula given by Anani *et al.* uses refractive indices of GaN and InN to calculate refractive index of $In_yGa_{1-y}N$ [19]. However, their studies lack complete data of InN and most of earlier available formulas of refractive index of InN are fitted by assuming bandgap of InN to be around 1.9 eV [15,20,21], which is actually around 0.7 eV [18]. We used the latest results of InN [22,23] into the formula of Anani *et al.* and found that the calculated refractive index of $In_yGa_{1-y}N$ is smaller than 2.3, which seems abnormal. Finally, we applied the energy shift method proposed by Bergmann *et al.* [24] and adopted E_g from [18] to calculate refractive index of $In_yGa_{1-y}N$. E_g of $In_yGa_{1-y}N$ is:

$$E_g(y) = 0.7y + 3.45(1-y) - 1.4y(1-y) \quad (5)$$

Refractive index of sapphire is calculated by the Sellmeier equation:

$$n(\lambda)^2 = 1 + A_1\lambda^2 / (\lambda^2 - \lambda_1^2) + A_2\lambda^2 / (\lambda^2 - \lambda_2^2) + A_3\lambda^2 / (\lambda^2 - \lambda_3^2) \quad (6)$$

where A_1, A_2, A_3, λ_1, λ_2, and λ_3 are fitting parameters obtained from [25].

Refractive index of ITO is calculated according to Cauchy function [26,27]:

$$n(\lambda) = B_1 + B_2 / \lambda^2 + B_3 / \lambda^4 \quad (7)$$

where B_1, B_2, and B_3 are fitting parameters. Experimental data from [28,29] are used to fit Eq. (7) to determine B_1, B_2, and B_3, which are 1.63632, 0.09713, and –0.00328, respectively.

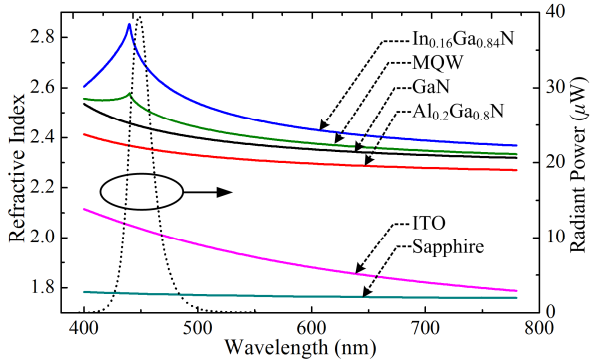

Fig. 2. Refractive indices of LED materials and the spectra of blue light (1 mW).

Calculated refractive indices of GaN, $Al_xGa_{1-x}N$, $In_yGa_{1-y}N$, sapphire, and ITO are shown in Fig. 2. In this study, molar fractions of x and y are set to be 0.2 and 0.16, respectively. Dopants in alloys are assumed to have slight impacts on refractive indices, and thus refractive indices of p-GaN and n-GaN are set to be the same as that of GaN, and refractive index of p-

#122383 - $15.00 USD Received 3 Feb 2010; revised 29 Mar 2010; accepted 5 Apr 2010; published 21 Apr 2010

AlGaN is equal to that of AlGaN. Refractive index of MQW layer is the mixing of refractive indices of GaN and InGaN by:

$$n_{\mathrm{MQW}} = (d_1 n_{\mathrm{InGaN}} + d_2 n_{\mathrm{GaN}}) / (d_1 + d_2) \tag{8}$$

where d_1 and d_2 are thickness of InGaN and GaN, respectively. This study sets d_1 and d_2 to be 3 nm and 7 nm, respectively.

2.2 Absorptions of blue LED materials

For GaN and AlGaN, since the optical energy of visible light is a little lower than their bandgaps, the light absorption is mainly affected by the defects and dopant concentration. The Urbach tail also shows slight contributions for the blue light absorption. In earlier studies [30–33], absorption coefficients of doped GaN and undoped GaN are normally higher than 10 mm^{-1} and 5 mm^{-1} due to the higher defects in their samples. After that, Ye *et al.* have tested the free carrier absorption in GaN with Si and Mg doped [34,35]. Their results show that the absorption coefficient of doped GaN is around 1-2 mm^{-1} by the free carrier absorption. Recent studies from Schad *et al.*, Hasegawa *et al.*, and Lelikov *et al.* reported that the absorption coefficients of doped GaN can be as low as 0.7 or 0.4 mm^{-1}, 1 mm^{-1}, and 2.3 mm^{-1}, respectively [36–38]. Oshima *et al.* have grown high quality GaN crystal and found the absorption of pure GaN crystal around 0.1 mm^{-1} [39]. Reports for the absorption of p-AlGaN are few. In earlier studies, the absorption coefficient of undoped AlGaN normally varies in the range of 8-25 mm^{-1} [32,40].

The light absorption in MQW layer is not clarity due to the large Stokes shift between the emission and the absorption, which is generated by the quantum confined Stark effect (QCSE) of piezoelectric and spontaneous polarization fields of quantum wells. QCSE broadens the absorption spectra and causes the emission spectra to be blue shift. O'Donnell *et al.* have analyzed the Stokes shift between the absorption and emission spectra of InGaN epilayer, and used a sigmoidal formula to describe the light absorption as following [41–43]:

$$\alpha = \alpha_0 / \{1 + \exp[(E_B - E) / \Delta E]\} \tag{9}$$

$$E_B = 0.993 + 0.719 E_P \tag{10}$$

where α is absorption coefficient of InGaN epilayer, α_0 is a fitting constant, E_B is the mean bandgap, E_P is the photon energy of emission peak, E is the photon energy of incident light, and ΔE is the absorption broadening factor equivalent to the Urbach tailing energy.

For InGaN/GaN MQW, two absorption edges are normally visible in the absorption spectra. One is located at the E_g of GaN, and the other is located at the E_B of InGaN. Equation (9) is effective to estimate the light absorption around the absorption edge of E_B. However, if the optical energy of incident light is beyond the blue light range, the value of Eq. (9) will be too low. We summarized the photoluminescence excitation data and measurement results from recent studies [44–48], and revised Eq. (9) to be Boltzmann form:

$$\alpha = \alpha_1 + (\alpha_0 - \alpha_1) / \{1 + \exp[(E_B - E) / \Delta E]\} \tag{11}$$

where α_1 is a fitting constant. In this study, α_0 and α_1 are set to be 5000 mm^{-1} and 5 mm^{-1}, respectively.

The light absorption of ITO strongly depends on the sputtering conditions and normally varies by the oxygen ratio in the growth [27–29]. This study assumes the oxygen ratio to be 10% and fits the absorption of ITO with data from [27]:

$$\alpha = 4\pi(C_1 / \lambda + C_2 / \lambda^2 + C_3 / \lambda^3 + C_4 / \lambda^4) \tag{12}$$

where the parameters C_1, C_2, C_3, and C_4 are fitted to be 0.28147, –0.34242, 0.14236, and –0.01916, respectively.

#122383 - $15.00 USD Received 3 Feb 2010; revised 29 Mar 2010; accepted 5 Apr 2010; published 21 Apr 2010

Sapphire is considered to be transparent for visible light. The buffer layer is assumed to be a high absorbing layer due to the high defects and dislocations during epitaxy. Schad *et al.* have estimated the absorption coefficient of the buffer layer to be approximately 390 mm^{-1} at wavelength of 430 nm [36].

As a summary, Fig. 3 shows the absorption data of LED materials from references and our calculations. Since the empirical formulas for the absorptions of doped GaN and doped AlGaN are not available, wide variation ranges are adopted in the following simulation for their absorptions in order to find the reasonable values. The ranges are 1-10 mm^{-1} for the GaN and 2-20 mm^{-1} for the AlGaN.

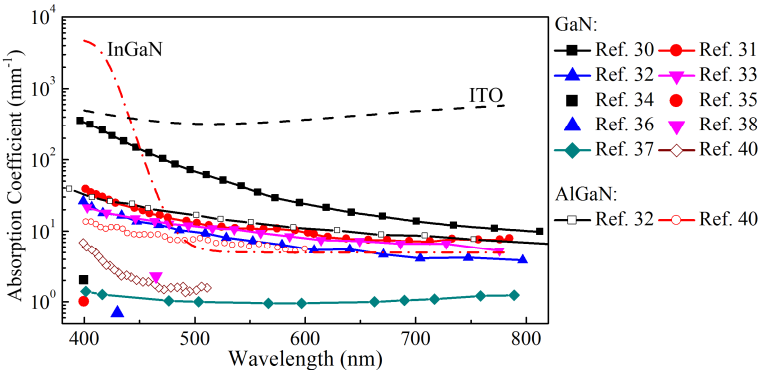

Fig. 3. Absorption coefficients of LED materials from references and our calculations.

2.3 Light scattering on nano-rough surfaces of blue LEDs

Our optical modeling only considers the light scattering on the external surfaces including the top surface and the four lateral surfaces, and the reflecting interfaces. From Fig. 1, for the top surface and the reflecting interface, four materials should consider their surface roughnesses: p-GaN (reflecting interfaces of flip chip and vertical injection chip), n-GaN (top surface of vertical injection chip), ITO (top surface of conventional chip), and sapphire (reflecting interface of conventional chip and top surface of flip chip). For the surface roughness of lateral surfaces, sapphire is specifically discussed due to its thick thickness, and ITO and GaN based materials are assumed with the same roughness.

Generally, the above mentioned surfaces are very smooth and show nano-scale roughness if no special treatment is applied. The light scattering intensity on these surfaces is described by total integrated scattering (TIS). TIS is the ratio of the scattered light to the total reflected light [49,50]:

$$\mathrm{TIS} = 1 - \exp[-(4\pi\delta\cos\theta_0 / \lambda)^2] \tag{13}$$

where δ is the rms roughness of surface, θ_0 is the angle of incident light.

δ of p-GaN, n-GaN and ITO strongly depend on their fabrication processes and sample quality. p-GaN is grown by the epitaxy. In earlier epitaxial growth, surface of p-GaN can be very rough due to poor process control. With the advancement of epitaxy, surface quality of p-GaN has been improved, and its δ can be lower than 1 nm [51–53].

δ of n-GaN of vertical injection chip is normally high, because its surface is formed by laser lift-off and RIE. Both of the processes break the crystal and affect surface quality. By better control of the two processes, smaller δ can be realized within 4-14 nm [54–56].

δ of ITO also can be high. Figure 4a shows one earlier LED and one currently commercial LED with their δ varying from 54 nm to 9.8 nm. In most cases, by better control of oxygen flow and annealing temperature, δ of ITO can be limited in the range of 3–13 nm [29,57,58].

#122383 - $15.00 USD Received 3 Feb 2010; revised 29 Mar 2010; accepted 5 Apr 2010; published 21 Apr 2010

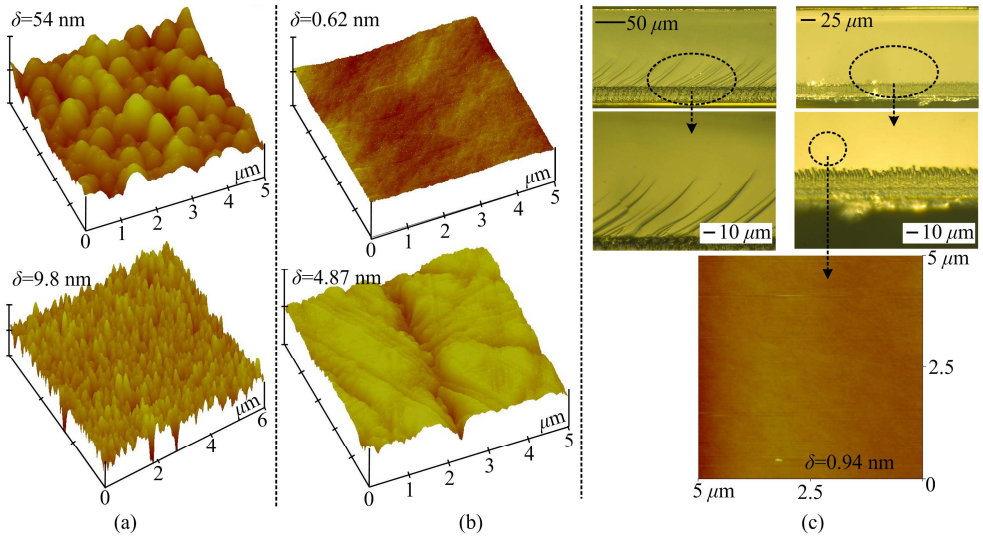

Fig. 4. Surface roughness of some commercial LED samples. (a) Top surface of ITO. (b) Top surface of sapphire. (c) Lateral surface of sapphire.

Surface of sapphire is generally polished by chemical mechanical polishing (CMP) before the sapphire using for the epitaxial growth. δ of the sapphire is normally lower than 1 nm in conventional chip [59]. For flip chip, the sapphire will be further polished before the dicing. Our group has shown that sapphire of flip chip can also realize mirror surface with δ lower than 1 nm [60]. But for some commercial LEDs, the surface of sapphire is a little rough, δ of which may be as high as 5 nm, as shown in Fig. 4b.

Figure 4c shows the lateral surface features of some conventional LEDs. In most cases, δ of lateral surface of the sapphire is below 1 nm, but some moiré like features at the bottom of the sapphire may increase the light scattering. δ of other lateral surfaces are higher. For ITO and GaN based materials, the lateral surfaces are formed by RIE and their δ may be higher than 4 nm. For the lateral surfaces of reflecting layer, bonding layer, and Si substrate, the modeling assumes their surface scattering as Lambertian scattering.

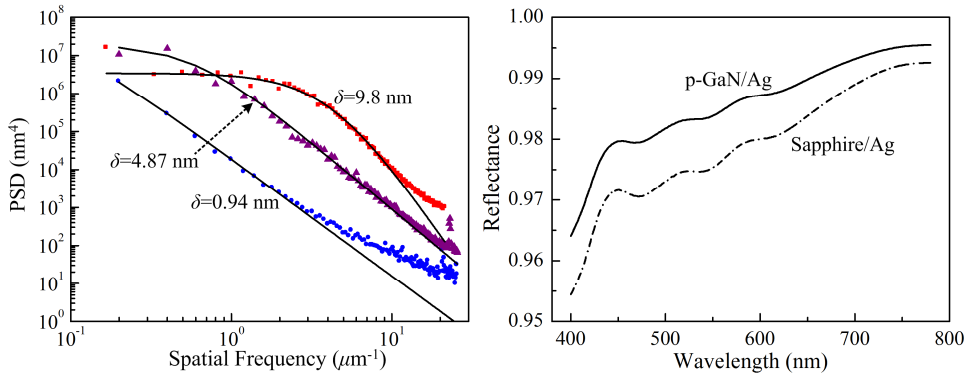

Fig. 5. (a) PSD functions from the tested AFM data of some rms roughness values. (b) Reflectance of Ag at the interfaces of p-GaN/Ag and sapphire/Ag. The solid lines in (a) are the fitting curves of *k*-correlation model.

After knowing the total scattering intensity by TIS, the next step is obtaining the angular scattering intensity of light on the nano-rough surfaces. A general numerical method used for the calculation of the angular scattering is converting the digitized roughness height from AFM data to the power spectral density (PSD) by Fourier transform, and then obtaining the BSDF over the whole solid angles [61–64].

#122383 - $15.00 USD Received 3 Feb 2010; revised 29 Mar 2010; accepted 5 Apr 2010; published 21 Apr 2010

$$\mathrm{PSD}(f_x, f_y) = \frac{1}{L^2}\left\{\sum_{m=1}^{N}\sum_{n=1}^{N} z_{mn} \times \exp[2\pi i \Delta L(f_x m + f_y n)](\Delta L)^2\right\}^2 \quad (14)$$

$$\mathrm{BSDF}(\theta_i, \theta_s) = (16\pi^2 / \lambda^4)\cos\theta_i \cos\theta_s Q(\theta_i, \theta_s)\mathrm{PSD}(f_x, f_y) \quad (15)$$

$$f_x = (\sin\theta_s \cos\phi_s - \sin\theta_i)/\lambda, \quad f_y = (\sin\theta_s \cos\phi_s)/\lambda \quad (16)$$

where L is the AFM scan length, z_{mn} is the profile height at coordinate of (m, n), N is the number of data points per line and row, $f_{x,y}$ is the spatial frequency at the x and the y direction, $\Delta L = N/L$ is the sampling distance, θ_i and θ_s are the angles of incident light and scattered light, φ_s is the azimuth angle of scattered light, and Q is the geometric mean of the sample specular reflectances at θ_i and θ_s (= $[R_s(\theta_i) \times R_s(\theta_s)]^{1/2}$).

Figure 5 shows the calculated PSD of some nano-rough surfaces. A k-correlation model (also called as ABC model) is used to fit the PSD data [65,66].

$$\mathrm{PSD}_{\mathrm{ABC}} = A/[(1 + B^2 f_{x,y}^2)^{(C+1)/2}] \quad (17)$$

where A is the magnitude at low $f_{x,y}$ values, B determines the position of the knee, and C is the slope at high $f_{x,y}$ values. K-correlation model has a relationship with δ as:

$$\delta^2 = 2\pi A/[B^2(C-1)] \quad (18)$$

We found that the k-correlation model shows good match with the tested PSD data and gives similar δ as those from AFM. In the following simulation, k-correlation model is also used to generate other PSD functions for δ that are not obtained from AFM test.

The final step is to determine the total reflectance and total transmittance on above nano-rough surfaces. For the transparent surfaces in terms of top surfaces and lateral surfaces, light is divided into transmitted light and reflected light. The transmittance and reflectance obey the Fresnel law. Diffuse parts of the transmitted light and reflected light have the same BSDF.

For the reflecting interfaces, both of specular reflection and diffuse reflection occur. Our optical modeling assumes Ag as the reflecting film. Total reflectance of Ag is:

$$R = \frac{1}{2}\left[\frac{(n_{\mathrm{Ag}} - n_i\cos\theta_i)^2 + k_{\mathrm{Ag}}^2}{(n_{\mathrm{Ag}} + n_i\cos\theta_i)^2 + k_{\mathrm{Ag}}^2} + \frac{(n_{\mathrm{Ag}} - n_i/\cos\theta_i)^2 + k_{\mathrm{Ag}}^2}{(n_{\mathrm{Ag}} + n_i/\cos\theta_i)^2 + k_{\mathrm{Ag}}^2}\right] \quad (19)$$

where n_i is the refractive index of sapphire or p-GaN, n_{Ag} and k_{Ag} are the real and imaginary refractive indices of Ag. Data of n_{Ag} and k_{Ag} covering the visible range are obtained from [67]. R for normal incidence is shown in Fig. 5.

Optical parameters of lateral surfaces of the reflecting layer and the bonding layer are 20% absorption, 50% specular reflection, and 30% Lambertian diffuse scattering. Reflectance of lateral surfaces of Si substrate in vertical injection chip is 50% specular reflection and 10% Lambertian diffuse scattering.

3. Monte Carlo ray-tracing simulation and experiment for bare blue LEDs

Based on the optical characterizations of the blue LEDs, Monte Carlo ray-tracing simulation was conducted with four cases considered, as shown in Table 1. In each of the first three cases, all of the surfaces are assumed with nanoscale roughness. Rms roughnesses of Sapphire/Ag and p-GaN/Ag are set to be 1 nm and 3 nm, respectively. Rms roughnesses of the lateral surfaces are 1 nm for the sapphire and 5 nm for other layers. Roughnesses of the top surfaces are changed as shown in Table 1. From Case I to Case III, the absorption coefficients of doped GaN and doped AlGaN vary from low absorption to high absorption as the above stated. For Case IV, surface roughness is not considered as the representative of previous studies.

#122383 - $15.00 USD Received 3 Feb 2010; revised 29 Mar 2010; accepted 5 Apr 2010; published 21 Apr 2010

During the ray-tracing simulation, photons are randomly generated from the MQW layer with their wavelengths in the range of blue spectra, as shown in Fig. 2. The total number of rays is 4,000,000, and the threshold is 10^{-5}. Light extraction efficiency and the radiation pattern are obtained from the simulation results.

After the ray-tracing simulation, commercial samples of conventional chip and flip chip were tested by HAAS-2000 spectroradiometer and GO1900L goniophotometer from Everfine. Since commercial samples for vertical injection chip with the top surface having nanoscale roughness is not available, we have to use a standard Lambertian pattern to compare with the radiation pattern of the simulated LEDs.

Table 1. Simulation Cases for Bare Blue LEDs

Cases	Absorption Coefficient (mm^{-1})	Rms Roughness (δ) of Top Surface (nm)		
		Conventional Chip	Flip Chip	Vertical Injection Chip
Case I	$\alpha_{GaN} = 1$, $\alpha_{AlGaN} = 2$	4-12	1-5	4-12
Case II	$\alpha_{GaN} = 5$, $\alpha_{AlGaN} = 10$	4-12	1-5	4-12
Case III	$\alpha_{GaN} = 10$, $\alpha_{AlGaN} = 20$	4-12	1-5	4-12
Case IV	α_{GaN}: 1-10, α_{AlGaN}: 2-20	0		

4. Monte Carlo ray-tracing simulation and experiment for packaged blue LEDs

A precise optical modeling of blue LEDs should also be capable of predicting the optical performance of packaged LEDs. LED samples above were packaged with silicone from Dow Corning and leadframe from local markers in China. Ray-tracing simulation for the packaged blue LEDs was conducted by using assumptions of Cases I and II for conventional chip and assumptions of Case I for flip chip according to simulation results of bare blue LEDs.

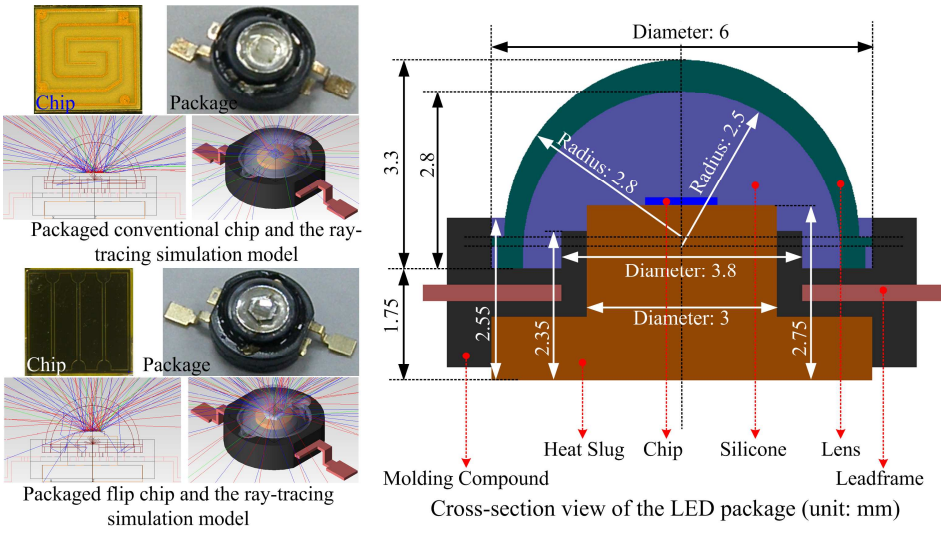

Fig. 6. Demonstration of experimental samples and ray-tracing models for packaged conventional chip and packaged flip chip, and illustration of the package structure.

Figure 6 shows the packaged samples and the structure of packaged conventional chip. Refractive indices of the silicone and the lens are 1.54 and 1.59, respectively. Surfaces of the leadframe and the heat slug are assumed to be coated with Ag. Optical parameters of these Ag coatings are 15% absorption, 60% specular reflection, and 25% Lambertian diffuse reflection. Reflectance of the black molding compound is set to be 20% with Lambertian diffuse pattern. The difference between the structures of packaged flip chip and packaged conventional chip is

#122383 - $15.00 USD Received 3 Feb 2010; revised 29 Mar 2010; accepted 5 Apr 2010; published 21 Apr 2010

that flip chip is bonded on a hexangular silicon submount before bonding on the heat slug. Thickness of the submount is 0.15 mm, and radius of its inscribed circle is 0.75 mm. Optical parameters of the submount are 30% absorption, 40% specular reflection, and 30% Lambertian diffuse reflection.

5. Results and Discussion

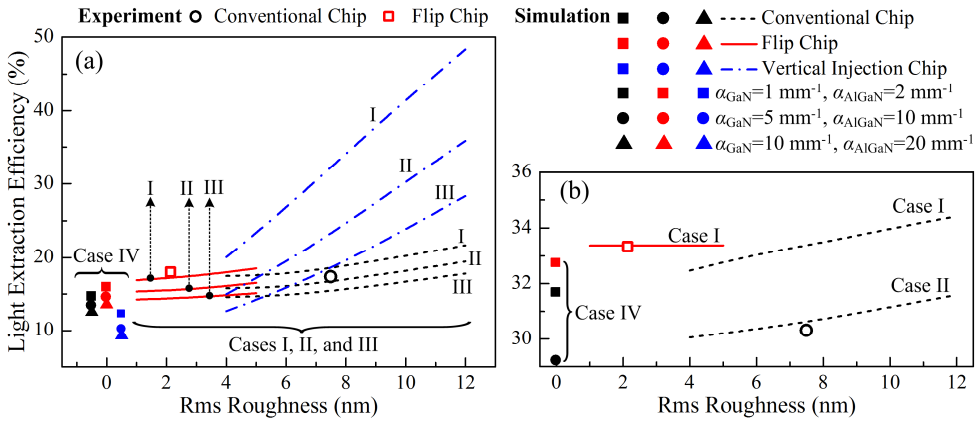

Fig. 7. Comparisons of light extraction efficiencies between the simulation and the experiment for (a) bare blue LEDs and (b) packaged blue LEDs.

Light extraction efficiencies of the bare blue LEDs are shown in Fig. 7a. It can be found that light extraction efficiencies for LEDs considering the surface roughness are higher than those without considering the surface roughness, especially for vertical injection chip. The difference can be as high as 7.06% for conventional chip, 2.61% for flip chip, and 36.12% for vertical injection chip.

In addition, with the increase of the surface roughness of the top surface, the light extraction efficiency is enhanced. Increments of the light extraction efficiency for conventional chip and flip chip are smaller than those for vertical injection chip, because the surface ratio of the top surface to the lateral surface for vertical injection chip is larger than those of conventional chip and flip chip.

Light extraction efficiency of the bare blue LED also strongly depends on the absorption coefficients of GaN and AlGaN. When the absorption coefficients change from Case I to Case III, the decreases of the light extraction efficiency are as high as 3.85% for conventional chip, 3.41% for flip chip, and 19.99% for vertical injection chip.

To determine the correction of our optical modeling, simulation results are compared with experimental results, as shown in Fig. 7a. Surface roughnesses of the commercial samples are tested by choosing some areas and determined by using the average values. The average rms roughnesses of the top surface are 7.52 nm for conventional chip and 2.16 nm for flip chip. Light extraction efficiencies of the commercial samples are determined by dividing the tested wall plug efficiencies by the internal quantum efficiency. Generally, the internal quantum efficiency of blue LEDs is around 70%. The tested wall plug efficiencies are 12.09% for conventional chip and 12.52% for flip chip. Therefore, the light extraction efficiencies are 17.27% for conventional chip and 17.88% for flip chip.

From Fig. 7a, larger differences are found between the results of Case IV and the experimental values of conventional chip and flip chip. The highest precision of Case IV (simulation/experiment) is around 88%. In our opinions, the simulation precision should not be lower than 95%. Comparing with Case IV, other cases with surface roughness considered show smaller differences between the simulations and experiments. The experimental value of flip chip is slightly higher than the result of Case I, and the experimental value of conventional chip locates between the curves of Cases I and II. The precision (simulation/ experiment) are 96.91% for conventional chip under Case II and 96.84% for flip chip under

#122383 - $15.00 USD Received 3 Feb 2010; revised 29 Mar 2010; accepted 5 Apr 2010; published 21 Apr 2010

Case I. Therefore, the surface roughness is critical for the precise optical modeling of bare blue LEDs.

For the absorption models, we cannot definitely declare that the absorption coefficients of GaN and AlGaN should be lower than 5 mm^{-1} and 10 mm^{-1} according to the results of Fig. 7a, because the material absorption strongly depends on the epitaxial and chip processes and can be even higher. But from our results, other designers will find the reasonable assumptions that can provide more precise models for present high brightness LEDs, most of which show better material quality and lower chip absorption. Taking our simulation as an example, if we want to improve the precision for bare LED to be higher than 99%, we only need to slightly adjust the absorption coefficients of GaN and AlGaN to be lower than present settings. But the adjustment sometimes is time consuming. Therefore, the designers should choose proper precision level for the optical modeling.

In previous simulations, comparing with conventional chip and flip chip, vertical injection chip did not show significant improvement of light extraction [12]. The improvement normally is due to the reduced chip absorption. But the slight improvement does not agree with the experiments. From Fig. 7a, due to the consideration of surface roughness, our optical modeling can show the change of light extraction by vertical injection chip. The increase of light extraction is twofold to threefold comparing with that of conventional chip, when the surface roughness is larger than 10 nm under Case I. This enhancement of light extraction is more reasonable and has been proved by many reports [55,68].

Figure 7b shows the comparisons of the simulation results and the experimental results for the packaged blue LEDs. Results reveal that our optical modeling is also capable of predicting the packaging performance when the surface roughness is considered. The precisions are as high as 98.89% (experiment/simulation) for conventional chip under Case II and 99.73% (simulation/experiment) for flip chip under Case I. It can be found that the precision of packaged LEDs is higher than that of bare LEDs. In addition, comparing Fig. 7a with Fig. 7b, dependences of light extraction efficiency on the surface roughness are different for bare LEDs and packaged LEDs. For conventional chip, the enhancement of light extraction efficiency is 4.21% for bare LEDs but 2.54% for packaged LEDs when the surface roughness increases from 4 nm to 12 nm. Flip chip also shows similar behaviors as the surface roughness increasing. What's more, light extraction efficiency of conventional chip shifts from the location of higher than Case II in Fig. 7a to the location of lower than Case II in Fig. 7b. The above differences are mainly due to the optical parameters of packaging components. In the experiments, factors such as the reflectance of mirror, chip location, size of lens, wettability of silicone on rough surface *et al.* all can affect the light extraction [69]. Therefore, the simulation precision of packaged LEDs can be adjusted by changing these factors. The importance of surface roughness for the precise modeling of packaged LEDs is weakened. From these findings, it can be deduced that a precise modeling of packaged LED may not have precise model of bare LED, but a precise modeling of bare LED is helpful to improve the precision of packaged LED.

Radiation patterns of the simulated LEDs are also compared with experiments. Both the radiation patterns of simulations and experiments are normalized to simplify their comparison. A normal cross correlation (NCC) function is used to evaluate the similarity of radiation patterns between the simulation and the experiment [2,9].

$$\mathrm{NCC} = \sum_i [I(\theta_i)_s - \bar{I}_s][I(\theta_i)_e - \bar{I}_e] \Big/ \sqrt{\sum_i [I(\theta_i)_s - \bar{I}_s]^2 \sum_i [I(\theta_i)_e - \bar{I}_e]^2} \qquad (20)$$

where $I(\theta_i)_s$ and $I(\theta_i)_e$ are the relative light intensity at angle θ_i for the simulation and the experiment, respectively; $\bar{I}_s$ and $\bar{I}_e$ are the mean values of $I(\theta_i)_s$ and $I(\theta_i)_e$ over the whole angles.

Similarities of radiation patterns between simulations and experiments are shown in Fig. 8 for the bare blue LEDs and Fig. 9 for the packaged blue LEDs. Results show that our optical modeling can also give precise description of the radiation patterns for both bare LEDs and

#122383 - $15.00 USD Received 3 Feb 2010; revised 29 Mar 2010; accepted 5 Apr 2010; published 21 Apr 2010

packaged LEDs. The simulation precisions are higher than 99% for bare LEDs and 98.5% for packaged LEDs. In Fig. 8, NCC values of conventional chip and flip chip are even larger than 99.5%.

From Fig. 8, it can be found that the relative light intensity of the simulation data is lower than that of the experimental data around the central angles for conventional chip and flip chip. In addition, a weak shoulder around the angle of 45° exists for the three types of LEDs. In Fig. 9, the shoulder shifts to the angle of 25° and the light emission converged into central angles, causing a sharp turning of the simulation data around the angle of 40°. By checking our optical models, we believed that the main reason causing the sharp shoulder is the sapphire layer. The difference of refractive indices between the sapphire and the silicone is smaller than that between GaN and the silicone, causing blue light to be more easily extracted from the lateral surfaces of the sapphire. On the other hand, location of the active layer is also important. Since the active layer is at the bottom or the top, thick sapphire enhances the side emission of packaged blue LEDs.

To diminish the shoulder, a reasonable approach is assuming the buffer layer with material scattering. In this layer, the dislocations and defects are serious and act as the scattering centers. Generally, sizes of these centers are smaller than the wavelength and cause the light to be scattered as the Rayleigh scattering. Therefore, part light generated from the active layer will be multiple reflected between the buffer layer and the p-GaN, meaning that less light enter the sapphire layer and emit from the lateral surfaces.

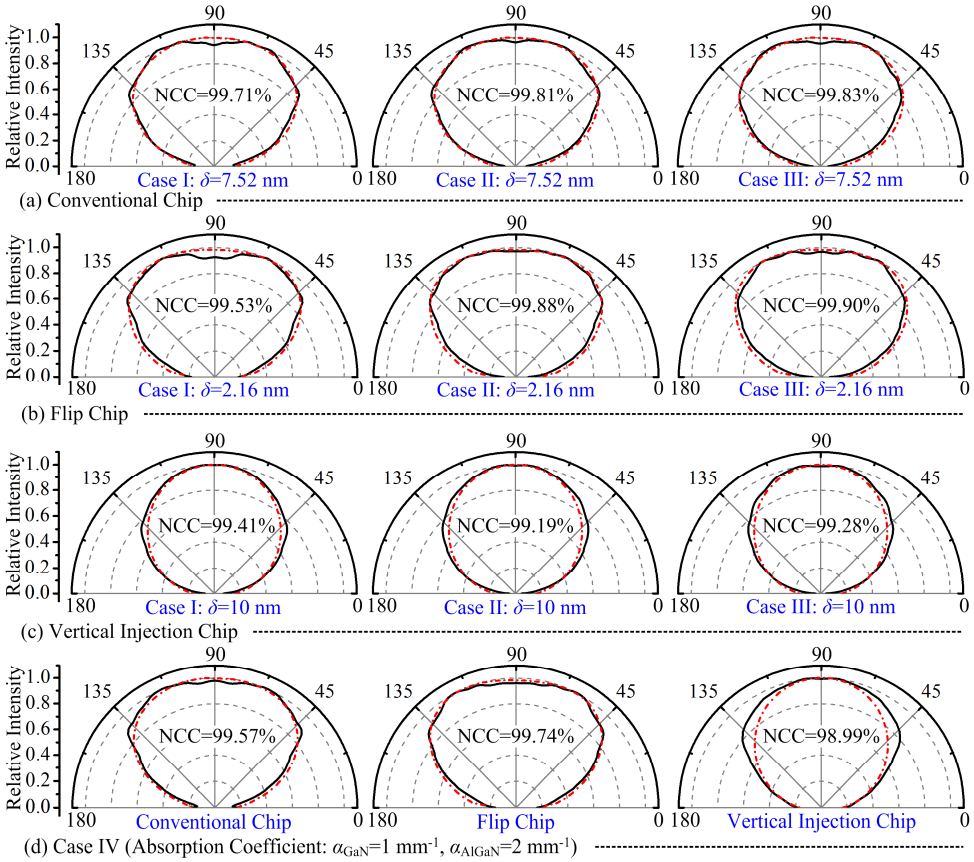

Fig. 8. Comparisons of radiation patterns between the simulation and the experiment for (a) conventional chip, (b) flip chip, (c) vertical injection chip, and (d) Case IV. The solid lines are the simulation results and the dashed lines are the experimental results.

#122383 - $15.00 USD Received 3 Feb 2010; revised 29 Mar 2010; accepted 5 Apr 2010; published 21 Apr 2010

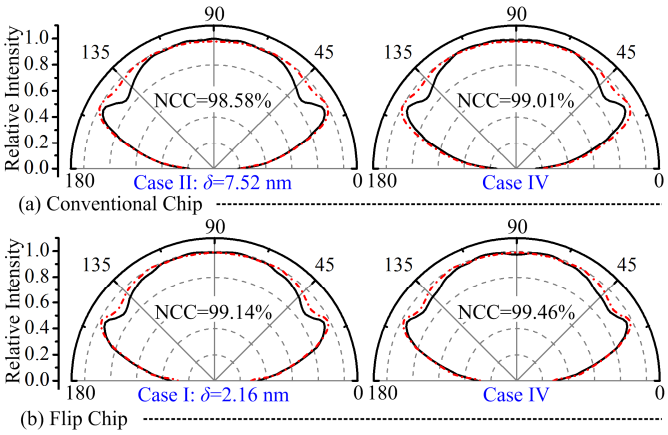

Fig. 9. Comparisons of radiation patterns between the simulation and the experiment for (a) packaged conventional chip and (b) packaged flip chip. The solid lines are the simulation results and the dashed lines are the experimental results.

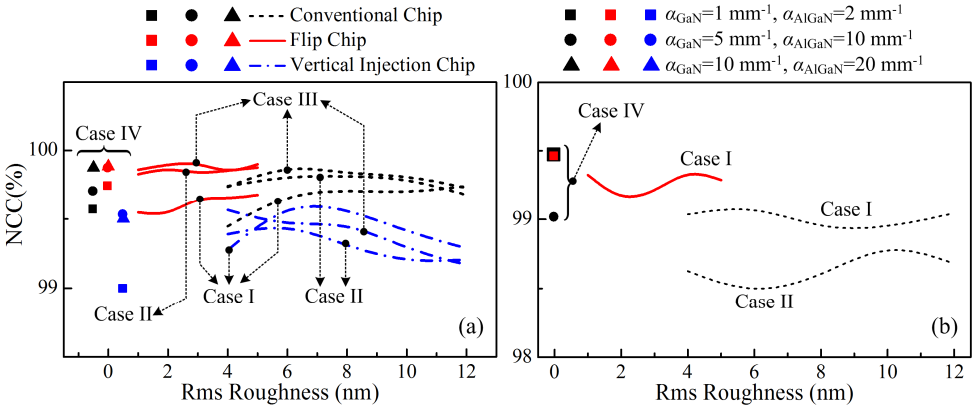

Fig. 10. Values of NCC of the radiation pattern between the simulation and the experiment for (a) bare blue LEDs and (b) packaged blue LEDs.

From Fig. 8, it also can be found that the variations of NCC are small for all of the three types of LEDs from Case I to Case III. The variations generally are not larger than 0.5%. This means that the dependence of normalized radiation pattern on the absorption coefficients of GaN and AlGaN is not strong. In addition, the changes of NCC values are small from Cases I, II, and III to Case IV. This may be due to the surface roughness of our study that is only nano-scale and cannot change the normalized radiation pattern significantly. However, it should be noticed that the absolute light intensity strongly depends on the chip absorption and the surface roughness due to their effects on the light extraction.

Figure 10 is a collection of the NCC values for both bare LEDs and packaged LEDs. It can be found that the variations of NCC are irregular as the surface roughness increasing. NCC of Case IV sometimes may be higher than that of other Cases. This irregularity may be due to the simulation errors and the test errors. However, it can be found that the overall variations are very small. Comparing the NCC values themselves, the variations almost can be negligible. If we take the absolute light intensity into consideration, real radiation patterns of the simulation results will clearly show their differences due to their differences on the light extraction. Higher light extraction means larger absolute light intensity. Therefore, only the light extraction can be precisely predicted, the real radiation pattern of the simulation can be close to that of the experiment. For Case IV, although the NCC value is high, the light extraction is lower than that of the experiment, causing the absolute light intensity of Case IV lower than

#122383 - $15.00 USD Received 3 Feb 2010; revised 29 Mar 2010; accepted 5 Apr 2010; published 21 Apr 2010

that of the experiment. For Case II of conventional chip and Case I of flip chip, although the NCC values sometimes are not the highest at the tested rms roughnesses, their real radiation patterns can show the best match with the experiments due to their higher precisions on the light extraction. From this view point, the surface roughness is also critical for the precise optical modeling of the radiation pattern.

6. Conclusion

Precise optical modeling of blue LEDs is constructed by assuming the refractive indices and the absorption coefficients of the chip materials with reasonable values from the references and applying the surface roughness in the optical modeling. Comparisons between simulations and experiments reveal that the surface roughness is critical for precise prediction of the light extraction and should be seriously considered in the optical modeling. Absorption coefficients of GaN and AlGaN depend on how the LED is fabricated and its chip structure, but possible values for those high brightness LEDs should be lower than 5 mm^{-1} and 10 mm^{-1}. The radiation pattern also can be precisely predicted by our optical modeling with the precision larger than 99% for bare blue LEDs and 98.5% for packaged blue LEDs.

Acknowledgement

This work was supported by the National Natural Science Foundation of China (NNSFC) Key Project under Grant 50835005, NNSFC Project under Grant 50876038, and High Technology Project of Ministry of Science and Technology under Grant 2008AA03A184. The authors thank the Science and Technology Department of Guangdong Province and Guangdong Real Faith Enterprises Group Co. Ltd for their support. The authors thank Han Yan, Pei Wang, and Bulong Wu for their technical supports.

#122383 - $15.00 USD Received 3 Feb 2010; revised 29 Mar 2010; accepted 5 Apr 2010; published 21 Apr 2010